Available online at www.sciencedirect.com
SCIENCE DIRECT®
Journal of Sound and Vibration 279 (2005) 817–841
JOURNAL OF SOUND AND VIBRATION
www.elsevier.com/locate/jsvi

Assessing tire forces due to roadway unevenness by the pothole dynamic amplification factor method

A.V. Pesterev[a], L.A. Bergman[b], C.A. Tan[c], B. Yang[d,*]

[a] *Institute for Systems Analysis, Russian Academy of Sciences, pr. 60-letiya Oktyabrya 9, Moscow 117312, Russia*
[b] *Aeronautical and Astronautical Engineering Department, University of Illinois at Urbana-Champaign, 104 S. Wright St., Urbana, IL 61801, USA*
[c] *Department of Mechanical Engineering, Wayne State University, 5050 Anthony Wayne Drive, Detroit, MI 48202, USA*
[d] *Aerospace and Mechanical Engineering Department, University of Southern California, 3650 McClintock Avenue, Los Angeles, CA 90089-1453, USA*

Received 28 February 2003; accepted 17 November 2003

Abstract

A technique is developed to assess the dynamic contact forces arising after passing road surface irregularities by a vehicle modelled as a general linear MDOF system. The equations governing vibration of a vehicle moving along an uneven profile are, first, transformed to the state-space form and, then, to a system of uncoupled first order complex differential equations. For a local roadway irregularity described functionally, solutions of all equations are found analytically and expressed in terms of a unique function of one complex variable, the so-called *pothole dynamic amplification factor*, which is specific to the irregularity shape. The solutions obtained are combined to give dependencies of the harmonic components of the contact forces arising after the passage of the irregularity on the vehicle speed and irregularity dimensions. The problem is shown to be decomposed into separate calculation of vehicle and pothole-specific data. The technique developed is not specific to a particular vehicle model or an irregularity shape: the vehicle model is represented by its mass, stiffness, and damping matrices, and the replacement of one irregularity by another simply requires replacement of one dynamic amplification factor function by another. The latter are derived in Appendix A for several pothole configurations. The discussion is amply illustrated by examples of the application of the technique to the calculation of the tire forces for two simple vehicle models and several potholes of different shape.

*Corresponding author. Tel.: +1-213-740-7082; fax: +1-213-740-8071.
E-mail addresses: pesterev@isa.ru (A.V. Pesterev), lbergman@uiuc.edu (L.A. Bergman), tan@wayne.edu (C.A. Tan), bingen@usc.edu (B. Yang).
URLs: http://www.aae.uiuc.edu/lndvl, http://www.eng.wayne.edu/people/tan.

0022-460X/$ - see front matter © 2004 Elsevier Ltd. All rights reserved.
doi:10.1016/j.jsv.2003.11.060

1. Introduction

The paper is concerned with the assessment of dynamic tire forces that arise after the passage of a road surface irregularity by a vehicle. The importance of this problem follows from the fact that typical road surface irregularities can result in large dynamic forces, which, in turn, considerably affect damage of the infrastructure (pavement or bridges), a significant portion of which in many countries is either aging or reaching the end of its life. The recently concluded multinational DIVINE project [1] noted that "trucks 'wear' pavements at a rate which is dependent not only on the static load carried by the vehicle, but also on the dynamic performance of the vehicle, on the longitudinal profile of the road and on the structural variability of the pavement". The outcomes of this project suggest that current understanding of the dynamic interactions between moving vehicles and the infrastructure carrying them is inadequate.

The effect of road surface irregularities on bridge vibration has been examined in many publications (see, e.g., Refs. [1–7] and references therein), and many methods for numerically solving the problem of a vehicle moving along a bridge with an uneven surface have been developed (e.g., Refs. [4–10]). As can be concluded from the results reported, as well as from our own numerical experiments, the main cause of high-magnitude bridge vibration is road unevenness. For example, high values (more than 100%) of the dynamic increment (DI) (defined as the ratio of the difference of the peak dynamic and static deflections to the peak static deflection) reported in some publications (e.g., Refs. [1–3]) cannot be explained if we assume a flat longitudinal profile of the bridge and its approaches. The report [1] states that "the surface profile of a bridge and its approaches are fundamental to the response of the truck suspension and in turn the dynamic response of the bridge" and notes further that "for a smooth profile, the influence of the truck suspension is insignificant". The main difficulty associated with this problem is in the large number of parameters involved. As a result, most studies are confined to extensive numerical modelling or field experiments. An obvious disadvantage of these approaches is that results of numerical or field experiments are often valid only for a particular bridge and vehicle and cannot easily be generalized to other configurations. It is then not surprising that results reported in the literature are sometimes contradictory (some examples of this kind are discussed in Ref. [11]).

In view of complexity of the problem of coupled bridge–vehicle vibration associated with a large number of parameters affecting the solution in a non-trivial way, it seems advisable to start our examination from certain typical isolated irregularities and to examine the problem of finding the vehicle response due to the passage of an irregularity located on the rigid foundation. To justify this point, we note that the local character of an irregularity suggests shortness of the passage time and, in view of considerable inertia of the bridge, its dynamics cannot be noticeably changed during that time. In addition, analysis of results of field and numerical experiments reported in the literature, as well as our numerical experiments, show that dynamic contact forces due to typical road surface irregularities are considerably greater than those caused by coupled bridge–vehicle vibration in the case of an ideally smooth road surface. Hence, neglecting the bridge dynamics, we find adequate approximations of the vehicle oscillations and dynamic forces that arise during, or immediately after, the passage of a short road surface irregularity. The effect of these additional forces on the bridge dynamics depends on their frequencies and magnitudes. Thus, in order to learn whether the bridge response can noticeably be affected by an irregularity, we basically need to know whether the vehicle eigenfrequencies match the fundamental frequency

of the bridge and whether the magnitudes of the corresponding harmonic forces due to the irregularity are sizeable.

The problem of calculation of the dynamic forces arising after passing an irregularity is very important, also, in studies related to pavement damage [1,12–15]. Based on experimental results reported in the literature, Potter et al. [15] conclude that the peak damage due to dynamic loads can be between 1.5 and 12 times the level of damage caused by a static load and note that, at highway speeds, "the parameter which causes the greatest variation in dynamic tire forces, and the largest changes in ranking of suspensions, is the road roughness level". Moreover, as indicated in Ref. [12], there is evidence that "fatigue failure of pavements is likely to be governed by peak dynamic forces, and not by the average dynamic forces". Then it follows that, both in bridge and pavement-damage related applications, it is critically important to establish how the peak tire forces depend on the irregularity dimensions, suspension characteristics, and vehicle speed.

The general idea of the approach discussed in this paper is the same as in the undamped case [11]: to decouple equations governing vibration of an MDOF vehicle model moving along an uneven road and to solve the uncoupled equations in the modal space. In the damped case, however, the governing equations cannot be uncoupled by direct transformation to the modal coordinates. Therefore, we first transform the system of second order governing differential equations to the state-space form. Then, solving the eigenvalue problem in the state space and representing the system response as a series in terms of vehicle eigenfunctions, we get an uncoupled system of first-order complex differential equations in modal coordinates. Note that the decoupling technique is, essentially, just an application of the conventional damped modal analysis to the problem under consideration. For a local irregularity described functionally, all equations are solved analytically, with the solutions being expressed in terms of a unique function of one complex variable, which is specific to a given shape of an irregularity. When transforming back to the physical space, the modal forces give rise to the Fourier components of the contact forces. No iterative procedures or numerical integration of the governing differential equations are involved, and all desired characteristics are calculated by analytical formulas.

The format of the presentation is as follows: In Section 2, the mathematical statement of the problem is given. In Section 3, the equations governing vibration of an MDOF vehicle moving along an arbitrary profile are, first, transformed to the state-space form and, then, reduced to an uncoupled system of first order complex differential equations in modal coordinates. For a local irregularity described functionally, these modal equations are solved analytically, which is discussed in Section 4. Sections 5 and 6 present the technique for the calculation of the Fourier components of the tire forces due to passing a local irregularity. Results of numerical experiments with simple vehicle models are presented and discussed in Section 7. Finally, pothole dynamic amplification factors for several potholes are derived in Appendix A.

2. Problem statement

Consider a vehicle model with n degrees of freedom and m contact points, schematically shown in Fig. 1. Let $z(t) \in \mathbb{R}^n$ be a vector of its physical coordinates such that $z(t) = 0$ corresponds to the equilibrium state and $z_c \in \mathbb{R}^m$ be a vector of vehicle coordinates (in the general case, linear combinations of the coordinates) that take part in the interaction with the ground. Denote by l_i,

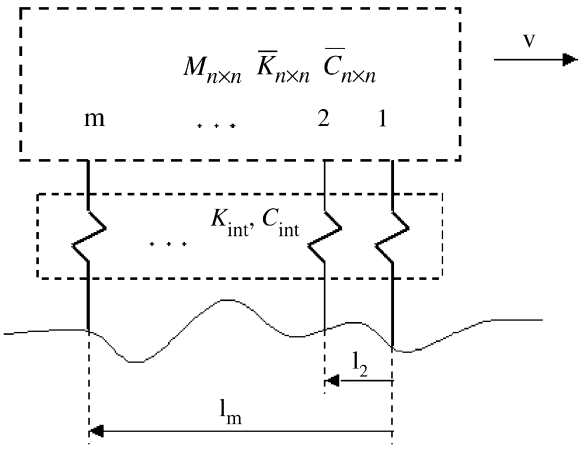

Fig. 1. A schematic of an MDOF vehicle moving along an uneven profile.

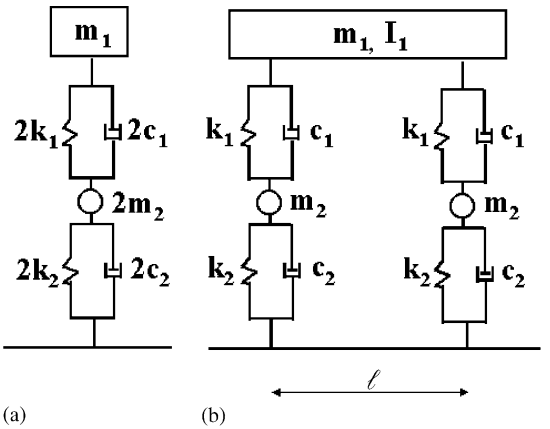

Fig. 2. (a) 2-DOF and (b) 4-DOF vehicle models.

$i = 1, \ldots, m$, the distance between the first and ith contact points, such that $l_1 = 0$ and $l_{i+1} - l_i$ is the distance between the $(i + 1)$th and ith contact points (axles). Let M be the mass matrix and $\bar{K}$ and $\bar{C}$ be stiffness and damping matrices of the free-free vehicle. Denote by S_v the $m \times n$ matrix that "chooses" contact coordinates, $z_c = S_v z$, and by K_{int} and C_{int} symmetric $m \times m$ matrices describing the interaction of the vehicle with the ground.

To exemplify the above notation, let us consider the "quarter-car" and "half-car" models depicted in Fig. 2 [6]. For the "quarter-car" model (Fig. 2(a)), we have $n = 2$, $m = 1$, $l_1 = 0$, $K_{\text{int}} = 2k_2$, $C_{\text{int}} = 2c_2$, and $S_v = [0, 1]$. For the "half-car" model (Fig. 2(b)), $n = 4$, $m = 2$, $l_1 = 0$, $l_2 = l$,

$$K_{\text{int}} = \begin{bmatrix} k_2 & 0 \\ 0 & k_2 \end{bmatrix}, \quad C_{\text{int}} = \begin{bmatrix} c_2 & 0 \\ 0 & c_2 \end{bmatrix}, \quad S_v = \begin{bmatrix} 0 & 0 & 1 & 0 \\ 0 & 0 & 0 & 1 \end{bmatrix}.$$

The vehicle mass, stiffness, and damping matrices are written in a standard way and not presented here. The order of numbering the coordinates can be easily understood from the form of the matrices S_v.

The vibration of the vehicle moving with a speed v along a road with longitudinal profile $r(x)$ is governed by the equation

$$M\ddot{z}(t) + C\dot{z}(t) + Kz(t) = S_v^{\mathrm{T}} K_{\mathrm{int}} S_r r(vt) + S_v^{\mathrm{T}} C_{\mathrm{int}} S_r \dot{r}(vt), \tag{1}$$

where $K = \bar{K} + S_v^{\mathrm{T}} K_{\mathrm{int}} S_v$ and $C = \bar{C} + S_v^{\mathrm{T}} C_{\mathrm{int}} S_v$ are the stiffness and damping matrices of the supported vehicle and S_r is the operator defined by $S_r r(x) = [r(x-l_1), r(x-l_2), \ldots, r(x-l_m)]^{\mathrm{T}}$.

Any road surface unevenness excites vehicle vibration and results in the appearance of dynamic components of the contact forces, which are given by

$$F_c(t) = K_{\mathrm{int}}(S_v z - S_r r(vt)) + C_{\mathrm{int}}(S_v \dot{z} - S_r \dot{r}(vt)), \quad F_c \in \mathbb{R}^m. \tag{2}$$

After passing an isolated irregularity, the vehicle freely vibrates and the vector of tire forces can be represented as a sum of harmonic components (with decaying amplitudes),

$$F_c(t) = \sum_{j=1}^{n} F_c^j(t), \quad F_c^j(t) = f_j \mathrm{e}^{\alpha_j t} \cos(\omega_j t + \varphi_j), \tag{3}$$

where α_j and ω_j are real and imaginary parts of the vehicle eigenfrequencies $\lambda_j = \alpha_j + \mathrm{i}\omega_j$. Our primary goal is to estimate the contribution of all harmonics in the resulting tire forces.[1]

In the undamped case, $\alpha_j = 0$, and it was quite reasonable to measure the dynamic effect of a pothole in terms of the amplitudes f_j of the harmonic forces [11]. The situation is more involved in the damped case, since the magnitude of the force reduces with time. In the case of light damping, it seems natural to consider the coefficient f_j as a measure of the "magnitude" of the jth force. We will use these coefficients, which are further referred to as Fourier coefficients, or amplitudes, of the harmonic forces to assess the effect of a pothole throughout this work. However, for a highly damped oscillator, the maximum magnitude of the contact force may be considerably lower than f_j because of the term $\mathrm{e}^{\alpha_j t}$ and the phase delay φ_j. Moreover, in the verification of the method and the codes implementing it by numerically modelling a vehicle passing a pothole, we can observe values of the contact force at any moment but cannot directly measure the quantity f_j and, thus, cannot check whether a priori estimates of f_j obtained by means of the technique being developed are correct. Note also that, in some applications (such as those related to road damage), peak values of the contact forces are of major interest. Hence, another candidate for the quantity in terms of which the contribution of the jth harmonic due to a pothole is to be measured is the maximum magnitude of the jth harmonic after passing a pothole, $\max_{t \geqslant T_p} |F_c^j(t)|$, where T_p is the time required to pass the pothole. In what follows, we will use both quantities to represent the effect of a pothole on the vehicle dynamics.

The technique based on the transformation to the modal coordinates, which was used in the undamped case [11], cannot be directly applied to the damped case as the three matrices M, K,

[1] It should be noted that, in certain applications, of interest are also peak tire forces during the passage of the pothole. However, in this case, the right-hand side of Eq. (2) cannot be represented as the sum (3) of the harmonics, and the technique to be discussed in the paper cannot directly be applied. Therefore, in this paper, we confined ourselves to calculating the response only after the pothole. The extension of the method to calculating peak tire forces in the pothole will be discussed in a future paper.

and C cannot, generally, be simultaneously diagonalized. In order to uncouple system (1), we need first to transform it to a system of first order differential equations in the state space.

3. Decomposition in the state space

By introducing the notation X for the state-space vector,

$$X(t) = \begin{Bmatrix} z(t) \\ \dot{z}(t) \end{Bmatrix} \in \mathbb{R}^{2n},$$

the governing equation (1) is written in the state space as

$$\dot{X} = AX + \tilde{F}, \tag{4}$$

where

$$A = \begin{bmatrix} 0_{n\times n} & I_{n\times n} \\ -M^{-1}K & -M^{-1}C \end{bmatrix},$$

$$\tilde{F} \equiv \tilde{F}_1 + \tilde{F}_2 = \begin{Bmatrix} 0 \\ M^{-1}S_v^{\mathrm{T}}K_{\mathrm{int}} \end{Bmatrix} S_r r(vt) + \begin{Bmatrix} 0 \\ M^{-1}S_v^{\mathrm{T}}C_{\mathrm{int}} \end{Bmatrix} S_r \dot{r}(vt).$$

Let $\Lambda = \mathrm{diag}[\lambda_1, \ldots, \lambda_n, \lambda_{-1}, \ldots, \lambda_{-n}]$, where $\lambda_{\pm k} \in \mathbb{C}$ are eigenvalues of the homogeneous equation (4), $\lambda_k = \alpha_k + \mathrm{i}\omega_k$. Denote by $\phi = [\phi_1, \ldots, \phi_n, \phi_{-1}, \ldots, \phi_{-n}]$ and $\psi = [\psi_1, \ldots, \psi_n, \psi_{-1}, \ldots, \psi_{-n}]$ matrices of the orthonormalized eigenvectors of A and A^{T} [16],

$$A\phi = \phi\Lambda, \quad A^{\mathrm{T}}\psi = \psi\bar{\Lambda}, \quad \psi^*\phi = 2I, \quad \psi^*A\phi = 2\Lambda,$$

where the bar and asterisk denote complex conjugate and adjoint quantities, respectively. It is well known [16] that $\lambda_{-k} = \bar{\lambda}_k, \phi_{-k} = \bar{\phi}_k$, and $\psi_{-k} = \bar{\psi}_k$.

Representing X in the form

$$X(t) = \tfrac{1}{2}\phi q(t),$$

where $q(t)$ is a $2n$-vector of modal coordinates, substituting it into Eq. (4), and premultiplying the equation obtained by ψ^*, we get the system of the uncoupled equations in q,

$$\dot{q} = \Lambda q + \psi^*\tilde{F},$$

or, in the coordinate-wise form,

$$\dot{q}_k = \lambda_k q_k + \psi_k^*\tilde{F}_1 + \psi_k^*\tilde{F}_2, \tag{5}$$

where $k = \pm 1, \ldots, \pm n$. By complex conjugation of Eq. (5), we find that $q_{-k} = \bar{q}_k$ and X is a real vector,

$$X = \frac{1}{2}\sum_{k=-n}^{n} \phi_k q_k = \frac{1}{2}\sum_{k=1}^{n} [\phi_k q_k + \overline{\phi_k q_k}] = \sum_{k=1}^{n} \mathrm{Re}[\phi_k q_k].$$

The contact forces are calculated as

$$F_c = [K_{\text{int}}, C_{\text{int}}]\left\{ \begin{bmatrix} S_v & 0 \\ 0 & S_v \end{bmatrix} X - \begin{bmatrix} S_r & 0 \\ 0 & S_r \end{bmatrix} \begin{Bmatrix} r(vt) \\ \dot{r}(vt) \end{Bmatrix} \right\}. \tag{6}$$

Thus, we have reduced the coupled equations (1) in the physical space to the system (5) of n uncoupled equations in modal coordinates $q_k(t)$. By introducing the notation

$$D_{k1} = \psi_k^* \begin{bmatrix} 0 \\ M^{-1} S_v^{\mathrm{T}} K_{\text{int}} \end{bmatrix}, \quad D_{k2} = \psi_k^* \begin{bmatrix} 0 \\ M^{-1} S_v^{\mathrm{T}} C_{\text{int}} \end{bmatrix}, \tag{7}$$

where D_{k1} and D_{k2} are complex vectors of length m, Eq. (5) is written in the form

$$\dot{q}_k = \lambda_k q_k + D_{k1,1} r(vt - l_1) + D_{k2,1} \dot{r}(vt - l_1) + \cdots + D_{k1,m} r(vt - l_m) + D_{k2,m} \dot{r}(vt - l_m). \tag{8}$$

Here $D_{k1,i}$ and $D_{k2,i}$ are the ith components of the vectors D_{k1} and D_{k2}, respectively.

4. Solution of the uncoupled equations for local irregularities

We now apply the decomposition obtained to the calculation of pothole-induced contact forces. By *pothole*, we mean a local irregularity; i.e., $r(x)$ is zero outside a certain finite interval $[x_0, x_0 + b]$. We will classify potholes in terms of their *shapes.* The latter is a function $\tilde{r}(x)$ that is defined on a fixed interval, vanishes at the endpoints of the interval,[2] and satisfies the condition $\max_{x',x''} |\tilde{r}(x') - \tilde{r}(x'')| = 1$. For definiteness, in this section, we assume that the shape function is defined on $[0, 1]$, although, in some cases (e.g., when $\tilde{r}(x)$ is a trigonometric function), it may be more convenient to consider functions $\tilde{r}(x)$ defined on different intervals, e.g., $[0, 2\pi]$ (see Appendix A).

Then, a particular pothole $r(x)$ located on an interval of length b is defined as $r(x) = a\tilde{r}((x - x_0)/b)$. The numbers a and $b > 0$ are referred to as the pothole "depth" and "width," respectively. By convention, $r(x) < 0$ corresponds to a depression in the road surface, and $r(x) > 0$ corresponds to an elevation in the profile. Two potholes $r_1(x)$ and $r_2(x)$ are said to be of the same shape if they can be described by means of one shape function $\tilde{r}(x)$; i.e., $r_1(x) = a_1\tilde{r}((x - x_{01})/b_1)$ and $r_2(x) = a_2\tilde{r}((x - x_{02})/b_2)$. In this case, they may differ by their *dimensions,* i.e., by width and depth.

We will be interested in the contact forces arising after passing a pothole. Denote by T_p the time required to pass the pothole. For $t > T_p$, Eq. (5) is homogeneous and describes the free vibration of an oscillator with eigenfrequency ω_k and damping coefficient α_k. The solution to this equation is

$$q_k(t) = q_k(T_p) \mathrm{e}^{\lambda_k (t - T_p)}, \quad t \geqslant T_p, \tag{9}$$

where $q_k(T_p)$ is the solution of the inhomogeneous Eq. (5) at $t = T_p$. Thus, we first need to find $q_k(T_p)$, the solution of Eq. (8) (or Eq. (5)) at $t = T_p$.

[2] Note that this requirement is not necessary and is assumed to simplify the notation. The resulting equations can easily be modified to adopt the case where $r(x_0 + b) \neq r(x_0)$ (different grades of the road before and after the irregularity).

4.1. Pothole dynamic amplification factor

For a given pothole $r(x)$, consider the complex-valued integral

$$I = \lambda \int_0^{T_p} \mathrm{e}^{\lambda(T_p-\tau)} r(v\tau)\,\mathrm{d}\tau \equiv a\lambda \int_0^{b/v} \mathrm{e}^{\lambda(b/v-\tau)} \tilde{r}(v\tau/b)\,\mathrm{d}\tau, \tag{10}$$

where λ is an arbitrary complex number. As can be seen, the value of this integral is determined by the shape $\tilde{r}(x)$ of the pothole and depends on four parameters: a, b, v, and λ, with the dependence on a being trivial. Let us show that the remaining three parameters are combined in one, such that the integral is a function of only one complex parameter. Indeed, denoting

$$\gamma = \frac{\lambda b}{v} \tag{11}$$

and changing the integration variable, $\tau = (b/v)\xi$, we get

$$I = a\frac{\lambda b}{v} \int_0^1 \mathrm{e}^{(\lambda b/v)(1-\xi)} \tilde{r}(\xi)\,\mathrm{d}\xi = a\gamma \int_0^1 \mathrm{e}^{\gamma(1-\xi)} \tilde{r}(\xi)\,\mathrm{d}\xi = a\Phi(\gamma), \tag{12}$$

where

$$\Phi(\gamma) = \gamma \int_0^1 \mathrm{e}^{\gamma(1-\xi)} \tilde{r}(\xi)\,\mathrm{d}\xi. \tag{13}$$

As can be seen, the integral I depends on only one parameter γ (not counting the linear dependence on a), which represents the combined effect of b, v, and λ. The complex-valued function $\Phi(\gamma)$ is specific to the pothole shape and is referred to as the *pothole dynamic amplification factor* (DAF). For a pothole shape described functionally, it can be obtained in an analytical, explicit, form (see, e.g., Appendix A). In the next two sections, we will show that solutions of all modal equations (5) for $t \geqslant T_p$ can be expressed in terms of this function. First, we solve Eq. (8) in the case of one contact point ($m = 1$).

4.2. The case of one contact point

In this case, D_{k1} and D_{k2} are scalars, and Eq. (8) takes the form (recall that, by definition, $l_1 = 0$)

$$\dot{q}_k = \lambda_k q_k + D_{k1} r(vt) + D_{k2} \dot{r}(vt), \quad k = 1, \ldots, n. \tag{14}$$

Clearly, the solution to Eq. (14) can be represented as

$$q_k(t) = D_{k1} q_{k1}(t) + D_{k2} q_{k2}(t), \tag{15}$$

where $q_{k1}(t)$ and $q_{k2}(t)$ are solutions to the complex differential equations

$$\dot{q}_{k1} = \lambda_k q_{k1} + r(vt), \quad \dot{q}_{k2} = \lambda_k q_{k2} + \dot{r}(vt). \tag{16, 17}$$

First, we will show that q_{k1} and q_{k2} are related to each other. Indeed,

$$q_{k1}(t) = \int_0^t \mathrm{e}^{\lambda_k(t-\tau)} r(v\tau)\,\mathrm{d}\tau, \tag{18}$$

$$q_{k2}(t) = \int_0^t e^{\lambda_k(t-\tau)}\dot{r}(v\tau)\,d\tau = \int_0^t e^{\lambda_k(t-\tau)}d[r(v\tau)]$$
$$= r(v\tau)e^{\lambda_k(t-\tau)}\Big|_0^t + \lambda_k\int_0^t e^{\lambda_k(t-\tau)}r(v\tau)\,d\tau = r(vt) + \lambda_k q_{k1}(t)$$

(by virtue of the condition $r(0) = 0$). Substituting $t = T_p = b/v$ and taking into account that $r(vT_p) = r(b) = 0$, we find that, for any pothole shape,

$$q_{k2}(T_p) = \lambda_k q_{k1}(T_p). \tag{19}$$

Substituting $t = T_p$ into Eq. (18), comparing the equation obtained with Eq. (10), and taking into account Eqs. (12) and (19), we obtain

$$q_{k2}(T_p) = a\Phi(\gamma_k) \quad \text{and} \quad q_{k1}(T_p) = \frac{a}{\lambda_k}\Phi(\gamma_k),$$

where γ_k is given by Eq. (11) upon substitution of λ_k for λ, and Φ is the pothole amplification factor (13).

Substituting these into Eq. (15) and denoting

$$D_k = \frac{D_{k1}}{\lambda_k} + D_{k2}, \tag{20}$$

we finally get

$$q_k(T_p) = aD_k\Phi(\gamma_k). \tag{21}$$

Remark 1. In the undamped case, the pothole DAF function shows how much the amplitude of the free vibration of the oscillator after passing the pothole is greater than the pothole depth [17, Eq. (10)]. Comparing this with Eq. (21) and treating aD_k as a complex pothole depth in the modal space, we arrive at the same interpretation as in the undamped case: $\Phi(\gamma_k)$ shows how much the response of the modal oscillator after passing the pothole is greater than the pothole depth, which explains the use of the term "pothole dynamic amplification factor" for this function.

4.3. Arbitrary number of contact points

In the general case of $m \geqslant 1$, the solution to Eq. (8) can be found as

$$q_k(t) = \sum_{i=1}^{m} q_{k,i}(t), \tag{22}$$

where $q_{k,i}(t)$ is a solution to the equation

$$\dot{q}_{k,i} - \lambda_k q_{k,i} = D_{k1,i}r(vt - l_i) + D_{k2,i}\dot{r}(vt - l_i), \quad i = 1, \ldots, m. \tag{23}$$

For $t \geqslant T_i$, where $T_i = b/v + l_i/v$ is the moment when the right-hand side of Eq. (23) vanishes, the solution to Eq. (23) describes the free vibration and, as shown in the previous section, is given by

$$q_{k,i}(t) = q_{k,i}(T_i)e^{\lambda_k(t-T_i)} = aD_{k,i}\Phi(\gamma_k)e^{\lambda_k(t-T_i)}, \tag{24}$$

where (cf. with Eq. (20))

$$D_{k,i} = \frac{D_{k1,i}}{\lambda_k} + D_{k2,i}.$$

For $t \geqslant T_p \equiv T_m$, where T_m is the time when the last contact point leaves the pothole, Eq. (24) is valid for any i, and, substituting it into Eq. (22), we get

$$q_k(t) = a\sum_{i=1}^{m} D_{k,i}\Phi(\gamma_k)\mathrm{e}^{\lambda_k(t-T_i)} = a\left[\sum_{i=1}^{m} D_{k,i}\mathrm{e}^{\lambda_k(l_m-l_i/v)}\right]\Phi(\gamma_k)\mathrm{e}^{\lambda_k(t-T_p)}.$$

Denoting $D_k = \sum_{i=1}^{m} D_{k,i}\mathrm{e}^{\lambda_k(l_m-l_i)/v}$, we get the representation (9) for $q_k(t)$ with $q_k(T_p)$ given by Eq. (21). Thus, we see that the values of the modal coordinates at the moment when the vehicle leaves the pothole in the case of several contact points are calculated by the same formula as in the case of one contact point; i.e., the case of several contact forces reduces to the case of one contact point. The basic difference, however, is that, in the former case, the complex number D_k depends on vehicle speed.

Thus, for $t \geqslant T_p$, the solutions $q_j(t)$ of the uncoupled system (5) are harmonic functions (9) with decaying amplitudes. The initial values $q_j(T_p)$ of all modal coordinates, given by Eq. (21), are obtained by means of the unique complex-valued function $\Phi(\gamma)$, as given in Eq. (13). The basic result of this section deserves to be formulated as a theorem.

Theorem 1. *For any local pothole $r(x)$ of width b and depth a, solutions of all uncoupled equations* (5) *are expressed in terms of a unique shape-specific function $\Phi(\gamma)$* (13) *of one complex variable as*

$$q_k(T_p) = aD_k\Phi(\gamma_k),$$

where $\gamma_k = \lambda_k b/v$ and

$$D_k = \sum_{i=1}^{m}\left(\frac{D_{k1,i}}{\lambda_k} + D_{k2,i}\right)\mathrm{e}^{\lambda_k(l_m-l_i)/v}. \tag{25}$$

5. Calculation of contact forces

For $t \geqslant T_p$, the vector of contact force $F_c(t)$ is represented as a sum (3) of harmonic functions with decaying amplitudes. Let us obtain explicit equations for the functions $F_c^j(t)$, which are calculated by Eq. (6) upon substitution of $X_j(t) = \frac{1}{2}(\phi_j q_j(t) + \bar{\phi}_j\bar{q}_j(t))$ for $X(t)$. Taking into account that $r(vt) = \dot{r}(vt) = 0$ for $t \geqslant T_p$, we get

$$F_c^j = [K_{\mathrm{int}}, C_{\mathrm{int}}]\begin{bmatrix} S_v & 0 \\ 0 & S_v \end{bmatrix} X_j \equiv [K_{\mathrm{int}}, C_{\mathrm{int}}]X_j^c, \tag{26}$$

where $X_j^c \equiv [z_c, \dot{z}_c]$ is the "contact" state vector of length $2m$, consisting of the contact coordinates and their time derivatives.

Now, note that the entries of the eigenvectors $\phi_j \in \mathbb{C}^{2n}, j = 1, \ldots, n$, are not independent; namely, for any $k = 1, \ldots, n$, we have $\phi_{j,k+n} = \lambda_j\phi_{j,k}$ (which follows from the form of the matrix A in Eq. (4)). Therefore, in what follows, we will use only the first storeys of the eigenvectors ϕ_j and

will keep the same notation for them; i.e., from now on, ϕ_j is the n-vector consisting of the first n coordinates of the "old" vector ϕ_j.

Introduce the notation $\phi_j^c \in C^m$ for the reduced ("contact") jth eigenvector, $\phi_j^c = S_v \phi_j$. Then, the vector X_j^c is written as

$$X_j^c = \frac{1}{2} \begin{Bmatrix} \phi_j^c q_j(t) + \bar{\phi}_j^c \bar{q}_j(t) \\ \lambda_j \phi_j^c q_j(t) + \bar{\lambda}_j \bar{\phi}_j^c \bar{q}_j(t) \end{Bmatrix}.$$

Substituting this into Eq. (26) and denoting

$$G_j = (K_{\text{int}} + \lambda_j C_{\text{int}}) \phi_j^c, \quad G_j \in \mathbb{C}^m, \tag{27}$$

we obtain

$$F_c^j = \tfrac{1}{2}(G_j q_j(t) + \bar{G}_j \bar{q}_j(t)) = \text{Re}\{G_j q_j(t)\}.$$

Introducing the notation $\Phi_j(b/v) \equiv \Phi(\gamma_j) \equiv \Phi(\lambda_j b/v)$ and taking into account Eqs. (9) and (21), we obtain

$$F_c^j = \text{Re}\{G_j D_j(v) a \Phi_j(b/v) e^{\lambda_j (t - T_p)}\} = a e^{\alpha_j (t - T_p)} \text{Re}\{G_j D_j(v) \Phi_j(b/v) e^{i\omega_j (t - T_p)}\}. \tag{28}$$

Denoting by $F_c^{j,i}$ the ith entry of the vector F_c^j (the jth harmonic component of the ith contact force) and by G_{ij} the ith entry of the vector G_j, representing the complex numbers as vectors on the complex plane,

$$G_{ij} = |G_{ij}| e^{i\varphi_{1ij}}, \quad D_j(v) = |D_j(v)| e^{i\varphi_{2j}}, \quad \Phi_j(b/v) = |\Phi_j(b/v)| e^{i\varphi_{3j}},$$

and taking the real part of the ith storey of the vector equation (28), we get the desired representation

$$F_c^{j,i}(t) = f_j^i e^{\alpha_j (t - T_p)} \cos[\omega_j (t - T_p) + \varphi_{ij}], \tag{29}$$

where the amplitude (Fourier coefficient) and phase angle of the jth component of the ith contact force are given by

$$f_j^i = a |G_{ij} D_j(v)| |\Phi_j(b/v)|, \tag{30}$$

$$\varphi_{ij} = \varphi_{1ij} + \varphi_{2j}(v) + \varphi_{3j}(b/v). \tag{31}$$

As can be seen from Eqs. (29)–(31), the dynamics of the vehicle after passing a pothole is completely determined by the constant matrix $G \equiv [G_{ij}]_{i,j=1}^{m,n} \equiv [G_1, \ldots, G_n]$, speed-dependent vector $D(v) \equiv [D_1(v), \ldots, D_n(v)]$, and function $\Phi(\gamma)$. Recall that the pothole DAF function is specific to the pothole shape and does not depend on vehicle parameters. It can be obtained in analytical form for a number of pothole shapes of interest in advance and be stored in a "library" of pothole DAF functions. On the other hand, the matrix G and vector $D(v)$ are specific to a given vehicle and can be used with any pothole. They are easily calculated by Eqs. (27) and (25) in terms of physical and modal parameters of the vehicle model and need to be determined once.

Then, the desired characteristics of the vehicle dynamics due to traversing a pothole are obtained as simply as multiplying the corresponding complex numbers. For example, to find the amplitude and phase angle of the jth harmonic component of the ith tire force for a given vehicle moving with a speed v_0 due to passing a pothole of width b_0 and depth a_0, we calculate the product $a G_{ij} D_j(v_0) \Phi_j(b_0/v_0)$, where $\Phi_j(b_0/v_0)$ is found by substituting $\lambda_j b_0/v_0$ for γ into the formula for the

DAF function $\Phi(\gamma)$ of the pothole. Then, the magnitude and the phase angle of the complex number obtained are the desired amplitude f_j^i and phase angle φ_{ij} of the tire force. Clearly, the response of any physical coordinate of the vehicle to a road irregularity can be obtained in a similar way.

As discussed in Section 2, another characteristic of interest is the maximum magnitude of the harmonic component of the contact force. Differentiating the right-hand side of Eq. (29) and equating the resulting expression to zero, we find that the maximum of the force occurs at the moment t^* given by

$$t^* = \begin{cases} -(\varphi_{ji} + \xi_j)/\omega_j, & \text{if } \varphi_{ji} + \xi_j \leqslant 0, \\ (\pi - \varphi_{ji} - \xi_j)/\omega_j, & \text{if } \varphi_{ji} + \xi_j \geqslant 0, \end{cases}$$

where $\xi_j = \arctan(\omega_j/\alpha_j)$. Taking into account that the force may take its maximum value at $t = T_p$ (when the vehicle leaves the pothole), we finally get

$$\max_{t \geqslant T_p} F_c^j(t) = f_j^i \max\left\{ |\cos \varphi_{ji}|, \mathrm{e}^{\alpha_j t^*} |\cos(\pi/2 + \xi_j)| \right\}. \tag{32}$$

As noted earlier, the basic difference between the cases of one and several contact points is that, in the former, D_k is a constant complex number, whereas, in the case of $m > 1$, it is a function of vehicle speed. From a computational standpoint, this makes no difference: in the codes, D_k is always calculated by Eq. (25), which is valid for any m, and the amplitudes (maxima) of the harmonic components of the contact forces are calculated by the same formulas, independent of the number of contact points. The dependence of D_k on the speed does make a difference when we want to graphically represent the results of computation. Indeed, in the case of one contact point, both the amplitudes and the maximum values of the harmonics depend only on parameter b/v (the dependence on the pothole depth a is trivial) and, hence, can be represented in one figure versus b/v. In the case of several contact points, these characteristics depend on two parameters (for a fixed vehicle model) b/v and v, which implies that one 2D figure is not sufficient. In addition, the forces at different contact points are generally different, which requires construction of families of figures for each contact point separately. The graphical representation of the computational results in the undamped case was discussed in Ref. [11], which can also be employed for damped models. In this paper, we confine our numerical illustrations to models with one contact point, however.

6. Multiple eigenfrequencies

Finally, we discuss modifications required when the system has repeated eigenfrequencies, which seems to be rather typical for real vehicles (e.g., if a vehicle has p identical axles, the multiplicity of the axle-hop eigenfrequency may be equal to p). Let $\lambda_{j_1} = \lambda_{j_2} = \lambda_j$ be two repeated eigenfrequencies. Adding together the two harmonic forces with the same frequency, which are given by Eq. (28), we obtain

$$F_c^j = F_c^{j_1} + F_c^{j_2} = a\mathrm{e}^{\alpha_j(t-T_p)} \operatorname{Re}\{[G_{j_1} D_{j_1}(v) + G_{j_2} D_{j_2}(v)]\Phi_j(b/v)\mathrm{e}^{\mathrm{i}\omega_j(t-T_p)}\},$$

where D_{j_1} and D_{j_2} are complex numbers (25) corresponding to the j_1th and j_2th eigenmodes and G_{j_1} and G_{j_2} are the corresponding columns of the matrix G. Then, it follows that the amplitude of the harmonic force corresponding to the repeated eigenfrequency is given by

$$f_j^i = a|G_{ij_1}D_{j_1}(v) + G_{ij_2}D_{j_2}(v)||\Phi_j(b/v)|,$$

i.e., we have to add complex numbers $G_{ij_1}D_{j_1} + G_{ij_2}D_{j_2}$ and only then take the absolute value of the number obtained rather than to add magnitudes of the addends. The extension of this result to the case of an arbitrary multiplicity of an eigenfrequency is straightforward.

7. Examples

In the examples below, we use a "cosine" pothole given by

$$r(x) = \begin{cases} -\frac{1}{2}a\left[1 - \cos^{2\pi x/b}\right], & 0 \leqslant x \leqslant b, \\ 0, & x < 0, x > b. \end{cases} \tag{33}$$

The DAF $\Phi(\gamma)$ (Section 4.1) for this pothole is derived in Appendix A.

7.1. Damped SDOF oscillator

For the first example, we consider the application of the technique discussed to the evaluation of the contact forces acting on the road from an SDOF damped oscillator due to passing a pothole (33). The complex argument γ of the pothole DAF function can be replaced by two real variables, e.g., magnitude $|\gamma| = \omega_0 b/2\pi v = f_0(b/v)$ and the modal damping ratio $\zeta = \alpha/\alpha_{cr}$, where f_0 is the undamped oscillator eigenfrequency in Hertz and α_{cr} is the critical damping. The dependence on the pothole depth a can be dropped by normalizing the dynamic force by the static force $F_{st} = ka$, where k is the spring stiffness. It can be shown that the vehicle-specific factor GD in Eq. (30) does not depend on $|\gamma|$. Hence, it follows that, for a given modal damping ratio, the dependence of the amplitude (maximum) of the contact force on all other parameters can be described by one curve. Thus, we can represent all results in one figure as a parameterized family of curves.

Fig. 3 depicts the family of plots showing the dependence of the normalized amplitude of the contact force on $|\gamma|$ for different values of ζ from zero to 40%. Similar plots for the maximum contact force are depicted in Fig. 4. The y-axis shows how much the corresponding factor is greater than the static force ka.

Fig. 5 shows several plots of the maximum contact force after passing a pothole for higher levels of damping (from 60% to 99%). The amplitudes are not presented, since they seem to have no physical sense for highly damped oscillators: as ζ tends to one, the peak value of the amplitude goes to infinity.

The examination of the results obtained shows that, for low damping (from 0 through approximately 30%), the maximum force reduces rapidly as the damping coefficient increases. For moderate damping (from 30% through 60%), the dependence of the maximum force on the damping coefficient is weak (when ζ varies between 40% and 60%, the maximum force is nearly

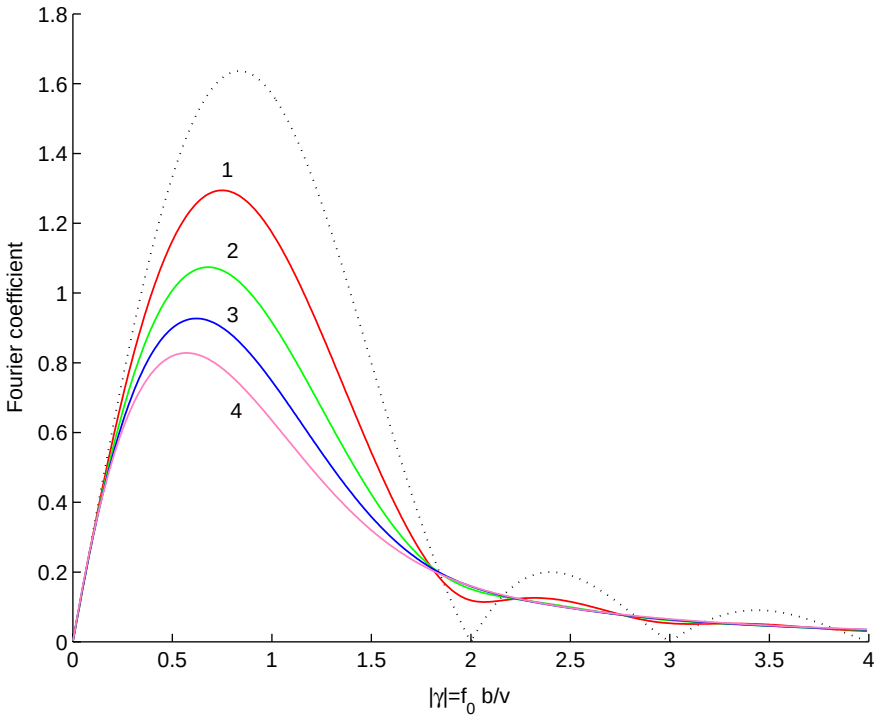

Fig. 3. Dependence of the amplitude of the normalized contact force on the oscillator eigenfrequency, speed, and pothole width for several values of damping ratio: $\zeta = 0$ (dotted line), $\zeta = 10\%$ (1), $\zeta = 20\%$ (2), $\zeta = 30\%$ (3), and $\zeta = 40\%$ (4).

constant). Starting from $\zeta = 60\%$, the maximum force increases with growth of the damping coefficient.

Another observation is that, for low and moderate damping, the maximum force, as a function of γ, has two local peaks. The left peak corresponds to the case where the force takes its maximum value at $t = T_p$, when the oscillator leaves the pothole. The right peak corresponds the case where the force takes its maximum value after the oscillator passes the pothole. For high levels of damping, the force always takes its maximum value at $t = T_p$, and the curves have only one peak.

7.2. Quarter-car model

We consider a quarter-car model depicted in Fig. 2(a) with the following parameters: $m_1 = 3.6 \times 10^4$ kg, $m_2 = 2.0 \times 10^3$ kg, $k_1 = 4 \times 10^6$ N/m, $k_2 = 1.2 \times 10^7$ N/m, $c_1 = 8.0 \times 10^4$ Ns/m, and $c_2 = 4.0 \times 10^4$ Ns/m. The body-bounce and axle-hop frequencies of the undamped (damped) model are 2.05 (2.05) Hz and 14.3 (13.3) Hz; the modal damping coefficients in the corresponding modes are 10% and 35%, respectively. The solid lines in Fig. 6 show the dependence of the "amplitudes" of the body-bounce (1) and axle-hop (2) forces on b/v. The dashed lines depict the maximum body-bounce (1) and axle-hop (2) forces. For the sake of comparison, the dotted lines

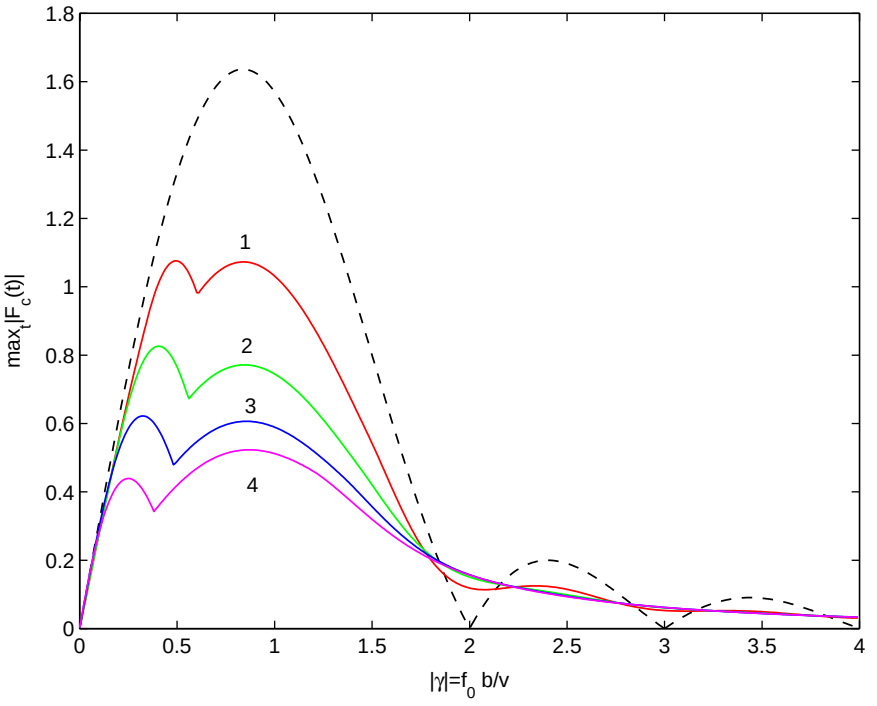

Fig. 4. Dependence of the normalized maximum contact force on the oscillator eigenfrequency, speed, and pothole width for several values of damping ratio: $\zeta = 0$ (dotted line), $\zeta = 10\%$ (1), $\zeta = 20\%$ (2), $\zeta = 30\%$ (3), and $\zeta = 40\%$ (4).

in the figure show the amplitudes of the body-bounce (1) and axle-hop (2) forces for the undamped model.

As can be seen, the incorporation of damping into the model reduces the contact forces, which is, of course, expected. It should be noted that the reduction in the axle-hop force is considerably greater than that in the body-bounce force, which is a general rule explained by the greater mass of the vehicle body compared to the axle mass.

The aim of the following experiment was to show that softening of the suspension stiffness (replacement of a steel suspension by an air suspension) increases the axle-hop force, which, in turn, explains (see Ref. [11] for detail) an interesting phenomenon reported in the DIVINE [1] report (regarding the replacement of a steel suspension by an air suspension resulting in an increase of the maximum response of a short-span bridge). The replacement of a steel suspension by an air suspension was modelled by reducing the spring coefficient k_1 by a factor of two, $k_1 = 2 \times 10^6$ N/m. All other parameters are unchanged. The eigenfrequencies of the new model are 1.54 and 12.3 Hz, and the corresponding damping ratios increased to 17% and 37%, respectively.

The dashed lines in Fig. 7 show the maximum body-bounce (1) and axle-hop (2) forces for the "steel-suspended" ($k_1 = 4 \times 10^6$ N/m) vehicle and are the same as those in Fig. 6. (Not to make the figure messy, the Fourier coefficients of the forces are not depicted). The solid lines correspond to the "air-suspended" ($k_1 = 2 \times 10^6$ N/m) vehicle. As can be seen, the body-bounce force in the

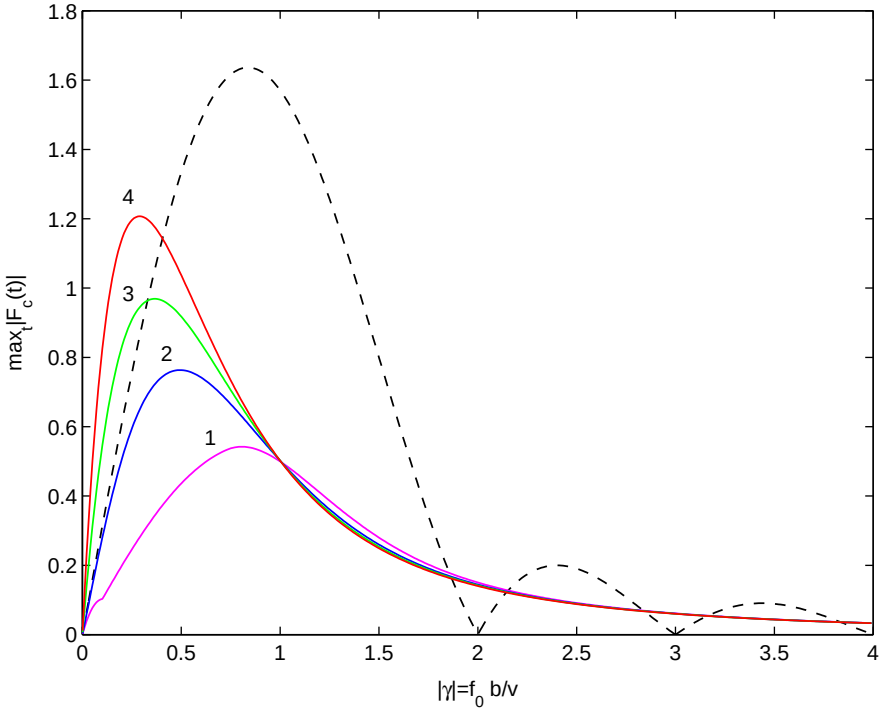

Fig. 5. Dependence of the normalized maximum contact force on the oscillator eigenfrequency, speed, and pothole width for several values of damping ratio: $\zeta = 0$ (dotted line), $\zeta = 60\%$ (1), $\zeta = 80\%$ (2), $\zeta = 90\%$ (3), and $\zeta = 99\%$ (4).

"air-suspended" model is considerably lower than that in the "steel-suspended" vehicle. However, the axle-hop force is increased (in spite of the fact that the axle-hop damping became slightly greater). This phenomenon is not specific to the particular model: the reduction of the suspension stiffness always increases the maximum axle-hop force, which is explained from the physical standpoint in Ref. [11]. Thus, the conclusion made in Ref. [11] that an air-suspended vehicle is potentially more dangerous for short-span bridges remains valid in the damped case.

It is generally accepted to consider air-suspended vehicles as "road-friendly". However, it follows from the above that the property of being "road-friendly" depends not only on the suspension stiffness and damping but also on the character of road unevenness. An air-suspended vehicle is road-friendly for a smooth road with long-wavelength irregularities but may not be road-friendly for a rough road surface with many short-wavelength potholes, which excite axle hop. To reduce the axle-hop, it is required to further increase suspension damping. These observations quite agree with DIVINE's conclusions based on field experiments: "Air suspensions do not necessarily have improved performance in the high-frequency axle modes and, again, require adequate damping" [1, p. 12].

Experiments (not presented) with variation of the suspension damper coefficient c_1 in the above-considered 2DOF model (with $k_1 = 4 \times 10^6$ N/m) showed that an increase of the damping above a certain level does not result in reduction of the dynamic loading. For example, when the

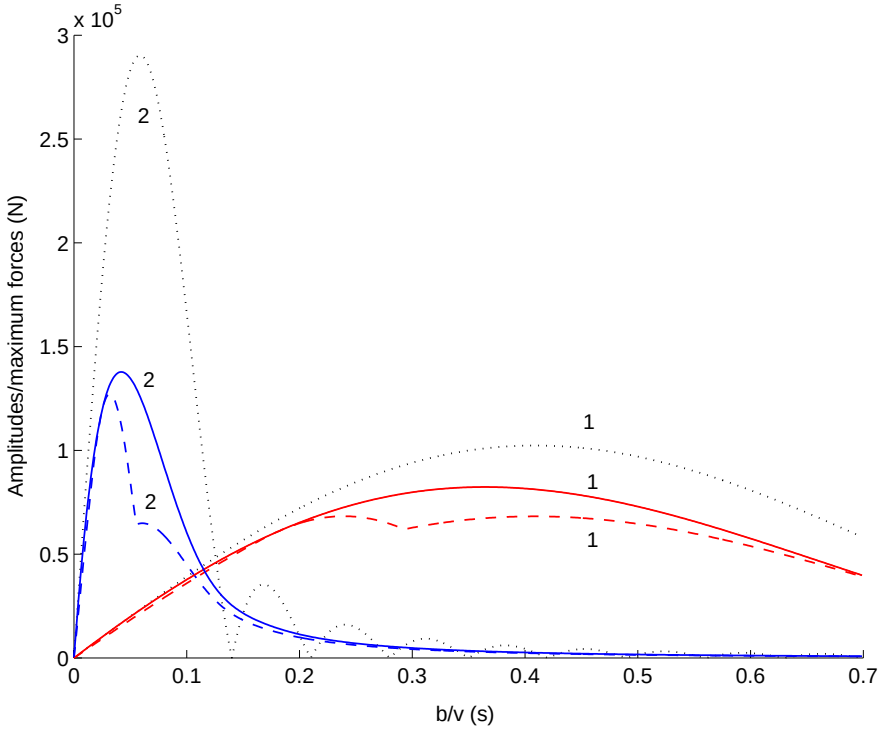

Fig. 6. Amplitudes (solid lines) and maximum values (dashed lines) of the body-bounce (1) and axle-hop (2) forces after passing a "cosine" pothole of depth $a = 1$ cm by the QC model. Dotted lines depict amplitudes of the body-bounce (1) and axle-hop (2) forces for the undamped model.

body-bounce modal damping in the above model increases from 20% to 25%, the reduction of the dynamic tire forces is very small. The increase of the damping ratio from 25% to 33% (for this value of the body-bounce modal damping, the axle-hop modal damping is equal to 100%) does not reduce the maximum contact forces. The results of these experiments agree with the conclusions reported in Ref. [1, p. 12].

7.3. *Comparison of the dynamic effects of different potholes*

7.3.1. *"Half-sine" pothole*

To illustrate the effect of the pothole shape on the vehicle dynamics, we considered a different—the so-called "half-sine"—pothole given by

$$r(x) = \begin{cases} -a \sin \dfrac{\pi x}{b}, & 0 \leqslant x \leqslant b, \\ 0, & x < 0, x > b. \end{cases} \tag{34}$$

Potholes (33) and (34) have the same width and depth but differ in their shapes. The basic difference is in their first derivatives near the pothole edges: function (33) is smooth, whereas the

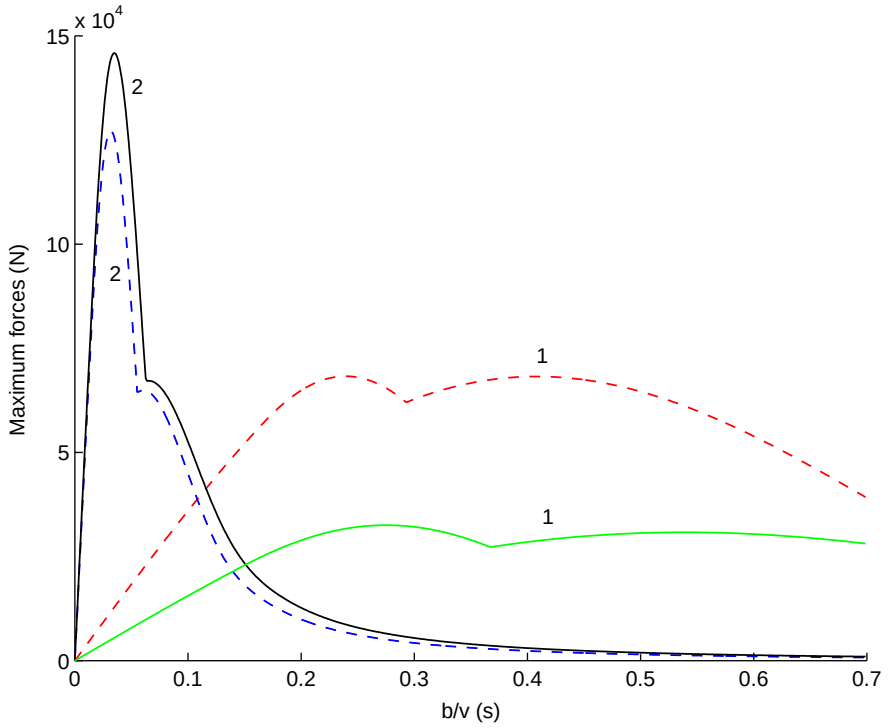

Fig. 7. The effect of the reduction of the suspension stiffness k_1 on the body-bounce (1) and axle-hop (2) forces. Dashed lines correspond to the "steel-suspended" model, and solid lines, to the "air-suspended" model.

first derivative of Eq. (34) has jumps at $x = 0$ and $x = b$. The function $\Phi(\gamma)$ (Section 4.1) for this pothole is derived in Appendix A.

Numerical experiments with an SDOF damped oscillator show that plots of both the Fourier coefficients and maximum contact forces look similar to those in the case of the "cosine" pothole. Figs. 8 and 9 demonstrate this for the oscillators with 30% and 60% damping (magnitudes of the pothole amplification factor functions in the undamped case for these two potholes were derived and compared in Ref. [17, Fig. 3]). In these figures, the curves showing amplitudes (solid lines) and maxima (dashed lines) of the contact forces corresponding to the "half-sine" pothole (34) are marked by 2, and those for the "cosine" pothole (33), by 1. Here, the x- and y-axis mean the same as in Figs. 3–5.

These figures, as well as results of other experiments with different damping coefficients (not presented), show that the peak values of the Fourier coefficient for the "half-sine" pothole occur at smaller values of the pothole width b (for a fixed speed v) or greater speeds (for a fixed pothole width) compared to the "cosine" pothole (i.e., the former are shifted to the left in the figures). As damping grows, this difference vanishes, such that, starting from about 40–50%, the peaks of both curves occur at approximately equal values of $|\gamma|$.

Another observation is that the peak values of the amplitudes and maxima of contact forces are always greater for the "half-sine" potholes than those for the "cosine" potholes, and the relative difference between them grows as the damping increases. This phenomenon seems to be explained

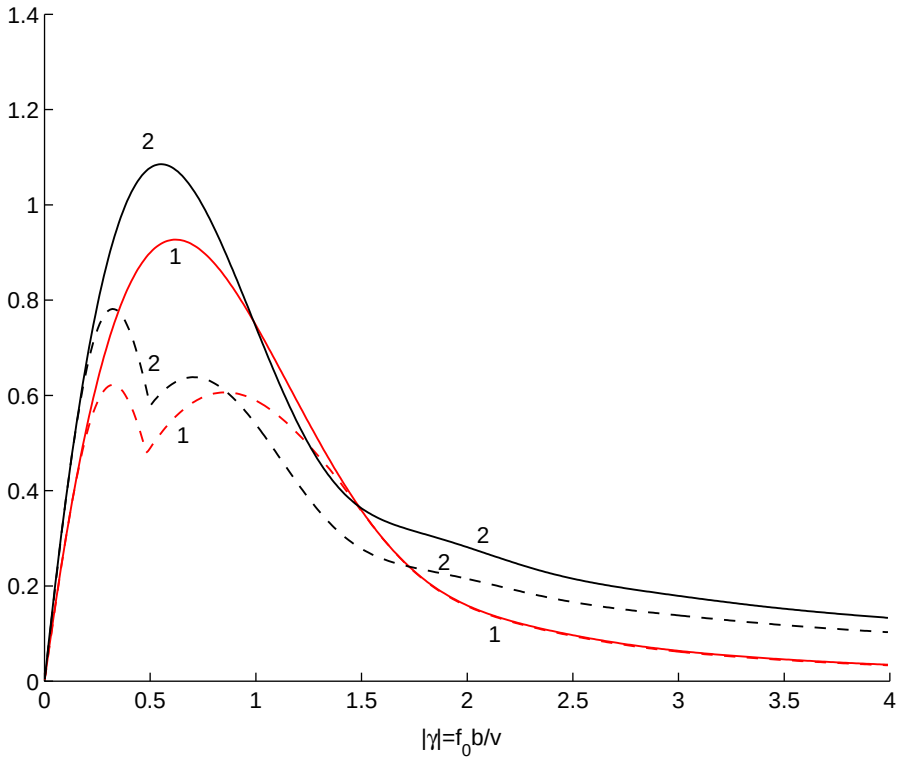

Fig. 8. Comparison of the amplitudes (solid lines) and maximum contact forces (dashed lines) due to passing "cosine" (1) and "half-sine" (2) potholes for an SDOF oscillator, $\zeta = 30\%$.

by the fact that the "half-sine" pothole has "steeper" edges (jumps in the slope), which results in higher damping forces. Since the contribution of the damping component in the total contact force increases with the growth of the damping coefficient, the last fact also explains why the contact force due to the "half-sine" pothole for highly damped oscillators (see, e.g., Fig. 9) is greater than that due to the "cosine" pothole for all values of $|\gamma|$.

7.3.2. "Polynomial" potholes

It is intuitively clear that the effect of a pothole on the dynamics of a vehicle traversing it should be determined by its "geometry configuration" rather than by a particular function used to approximate the pothole shape. To exemplify and justify this point, we consider two potholes described by polynomial functions, which were employed in numerical experiments in Ref. [7]. One is given by the second-degree polynomial (A.5); its shape is close to that of the "half-sine" pothole, and the slope at the ends has jumps. The other, described by the fourth-degree polynomial (A.7), has smooth edges and is similar in shape to the "cosine" pothole. Thus, one should expect that the effects of these potholes on a moving vehicle must be approximately equal to those due to the potholes (34) and (33), respectively.

The functions $\Phi(\gamma)$ for the fourth-degree and second-degree polynomial potholes are derived in Appendix A (Eqs. (A.8) and (A.6), respectively). The amplitude and maxima of the contact forces

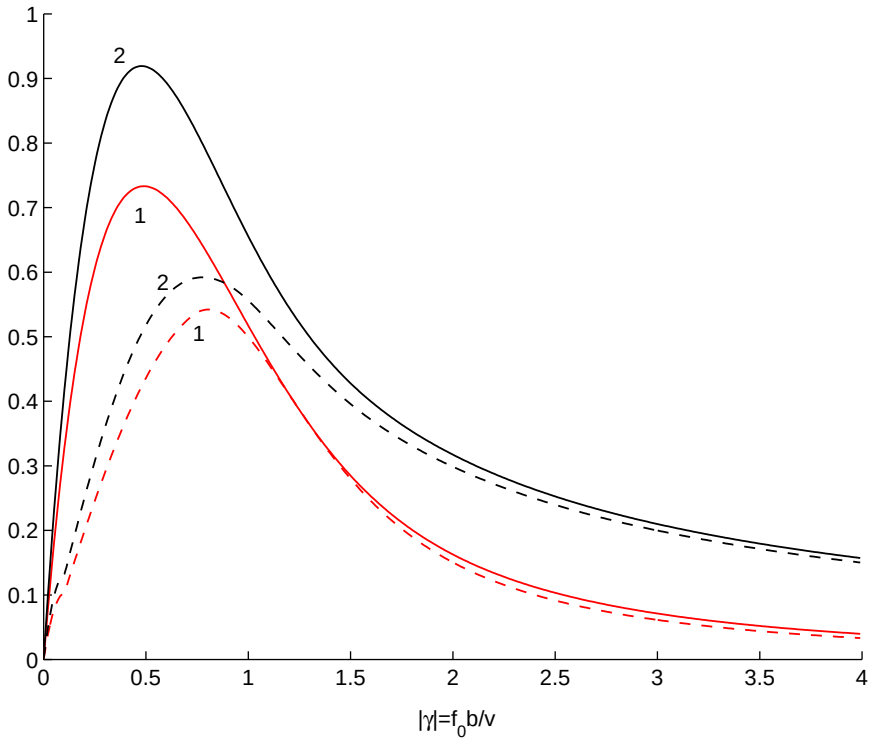

Fig. 9. Comparison of the amplitudes (solid lines) and maximum contact forces (dashed lines) due to passing "cosine" (1) and "half-sine" (2) potholes for an SDOF oscillator, $\zeta = 60\%$.

constructed by means of these functions for an SDOF oscillator with damping ratio 30% are shown in Figs. 10 and 11, respectively (curves marked by 2). These curves are compared with those obtained for the "cosine" (Fig. 10) and "half-sine" (Fig. 11) potholes, which are marked by *1*. (Note that, since functions for the trigonometric and polynomial potholes are given in terms of different γ (defined by Eqs. (A.1) and (11), respectively), the plots related to the latter were scaled along the x-axis by 2π.) As can be seen, the differences in the results for two pairs of the potholes compared are negligible from a practical standpoint.

The above implies that the dynamic effect of an irregularity is not sensitive to small variations in the shape functions as long as they do not considerably change the irregularity "geometry". In other words, if two different functions with similar smoothness conditions (e.g., both are differentiable or have equal jumps at the same set of locations) "adequately" approximate a pothole shape, it makes little difference which function is used for modelling the pothole. Since any functional description of a road irregularity is inevitably an approximation, it makes sense to confine the set of shape functions to several typical ones and create a "library" of pothole DAF functions. Then, if a given pothole can be approximated by a shape function from the library, we take advantage of the corresponding DAF function. If none of the "library" shape functions approximates well the pothole, we can introduce a new shape function and derive the pothole DAF function for it, extending, thus, the library.

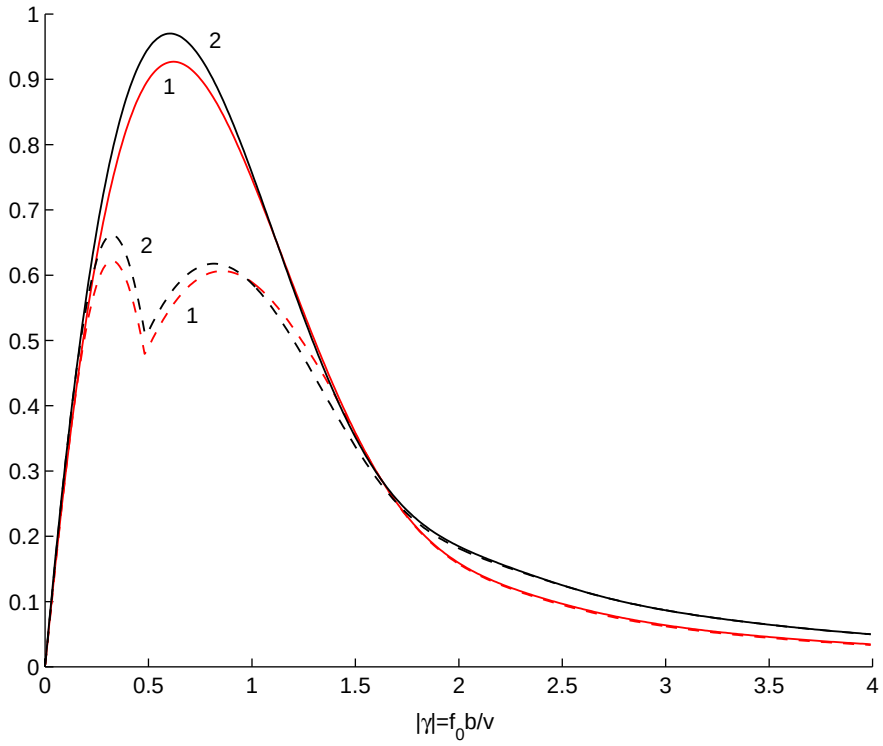

Fig. 10. Comparison of the amplitudes (solid lines) and maximum contact forces (dashed lines) due to passing "cosine" (1) and "4th degree polynomial" (2) potholes for an SDOF oscillator, $\zeta = 30\%$.

8. Conclusions

1. The technique for the decomposition of an arbitrary linear damped MDOF vehicle model moving along uneven road has been developed. It reduces the problem of vehicle vibration to solving independent complex first order differential equations.
2. For a local irregularity described functionally, all differential equations are solved analytically, with the solutions being expressed in terms of a unique complex-valued function, the so-called *pothole dynamic amplification factor*, specific to the pothole shape. Three parameters affecting the response of a modal oscillator—eigenfrequency, vehicle speed, and pothole width—are shown to be combined in one complex variable γ.
3. The pothole DAF method has been developed to assess harmonic components of the tire forces occurring after traversing a local road surface irregularity by a vehicle. The method reduces the problem to independent a priori calculation of vehicle-specific data and the pothole DAF function.
4. DAF functions have been derived for several typical pothole configurations.
5. The application of the method has been illustrated by numerical examples. For two simple vehicle models, plots of the magnitudes of the harmonic components of the contact forces arising after passing the "cosine" pothole (33) have been constructed, which show the dependence of these forces on the vehicle speed and pothole width.

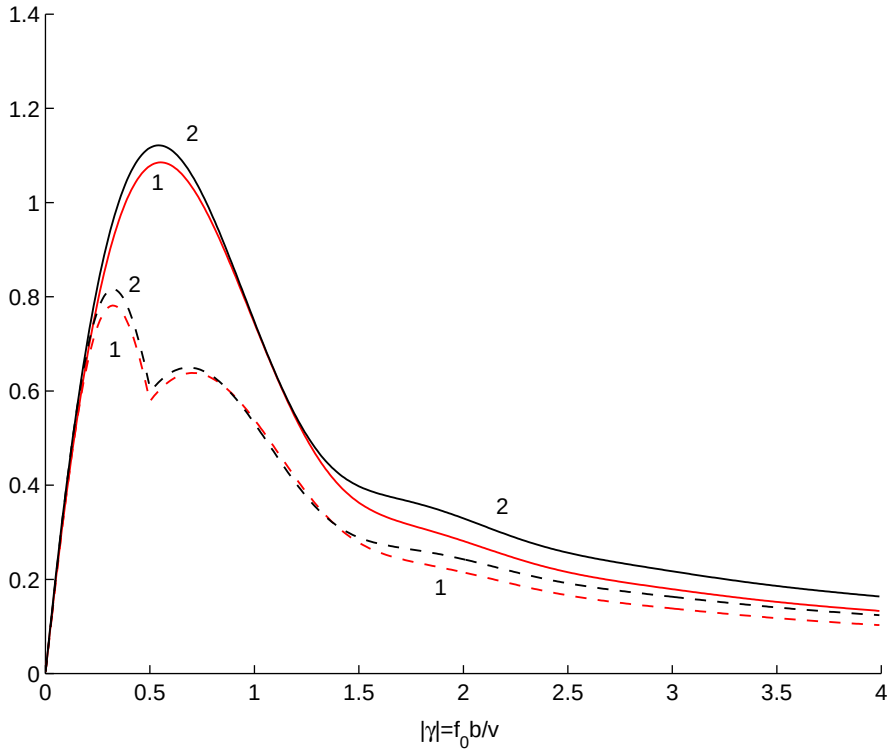

Fig. 11. Comparison of the amplitudes (solid lines) and maximum contact forces (dashed lines) due to passing "half-sine" (curves 1) and "2nd degree polynomial" (curves 2) potholes for an SDOF oscillator, $\zeta = 30\%$.

6. The technique is not specific to a particular shape of an irregularity. The replacement of one local irregularity by another requires simply replacement of one DAF function by another. It has been shown that the dynamic effect of a pothole is not sensitive to a particular function used to approximate its shape but is determined by its "geometric configuration".
7. The technique discussed has been applied to explain one interesting phenomenon reported in Ref. [1].
8. The technique can efficiently be used for design purposes. Letting any model parameters vary, one can immediately get a new family of plots showing dependencies of the magnitudes of the harmonic components of the contact forces on the vehicle speed and pothole sizes corresponding to the modified model and, thus, to easily observe the effect of the parameter variation on the vehicle dynamics.

Acknowledgements

The authors wish to acknowledge the support of the Civil and Mechanical Systems Division of the National Science Foundation through grant number CMS-9800136.

Appendix A. Pothole dynamic amplification factors for various potholes

As noted in the beginning of Section 4, for potholes described by trigonometric functions, it is more convenient to consider the domain $[0, 2\pi]$ rather than $[0, 1]$. For convenience of notation, we also redefine γ as (cf. Eq. (11))

$$\gamma = \frac{\lambda b}{2\pi v}. \tag{A.1}$$

Then, it can be checked directly that Eq. (13) for $\Phi(\gamma)$ takes the form

$$\Phi(\gamma) = \gamma e^{2\pi\gamma} \int_0^{2\pi} e^{-\gamma\xi} \tilde{r}(\xi)\, d\xi. \tag{A.2}$$

A.1. "Cosine" pothole

Substituting the shape function $\tilde{r}(\xi) = \frac{1}{2}(1 - \cos\xi)$ for the pothole (33) into Eq. (A.2) and taking the integral, we get

$$\Phi_c(\gamma) = \tfrac{1}{2}\gamma e^{2\pi\gamma} \int_0^{2\pi} e^{-\gamma\xi}(1 - \cos\xi)\, d\xi = \frac{\gamma e^{2\pi\gamma}}{2}\left\{ -\frac{e^{-\gamma\xi}}{\gamma} - \frac{e^{-\gamma\xi}}{\gamma^2 + 1}(-\gamma\cos\xi + \sin\xi) \right\}\Bigg|_0^{2\pi}.$$

Substituting the integration limits and simplifying, we obtain

$$\Phi_c(\gamma) = -\frac{1 - e^{2\pi\gamma}}{2(\gamma^2 + 1)}. \tag{A.3}$$

A.2. "Half-sine" pothole

The shape function for the pothole (34) is $\tilde{r}(\xi) = \sin\xi/2$. Substituting it into Eq. (A.2) and taking the integral, we get

$$\Phi_{hs}(\gamma) = \gamma e^{2\pi\gamma} \int_0^{2\pi} e^{-\gamma\xi} \sin(\xi/2)\, d\xi = \frac{\gamma e^{2\pi\gamma} e^{-\gamma\xi}}{\gamma^2 + \frac{1}{4}}\left(-\gamma\sin(\xi/2) - \tfrac{1}{2}\cos(\xi/2)\right)\Bigg|_0^{2\pi}.$$

Simplifying, we obtain

$$\Phi_{hs}(\gamma) = \frac{2\gamma(1 + e^{2\pi\gamma})}{4\gamma^2 + 1}. \tag{A.4}$$

A.3. Two "polynomial" potholes

Finally, we will get the dynamic amplification factor functions for two potholes considered in Ref. [7], which are described by polynomial functions. For these potholes, it is more convenient to take the interval $[0, 1]$ for the domain of the shape functions and introduce the parameter γ as in Section 4.1 (see Eq. (11)). The first pothole (with non-smooth edges) is described by the

polynomial of the second degree [7, Eq. (1)]:

$$\tilde{r}(\xi) = 4\xi - 4\xi^2, \quad 0 \leqslant \xi \leqslant 1. \tag{A.5}$$

Substituting this into Eq. (13), taking the integral by parts twice, and simplifying, we get

$$\Phi_{p2}(\gamma) = \frac{4}{\gamma}\left[(1 + e^{\gamma}) + \frac{2(1 - e^{\gamma})}{\gamma}\right]. \tag{A.6}$$

The shape of the second, "smooth", pothole is described by the fourth-degree polynomial [7, Eq. (2)]

$$\tilde{r}(\xi) = (2\xi - 1)^4 - 2(2\xi - 1)^2 + 1, \quad 0 \leqslant \xi \leqslant 1. \tag{A.7}$$

Substituting this into Eq. (13), taking the integral by parts four times, and simplifying, we get

$$\Phi_{\mathrm{p4}}(\gamma) = -\frac{32}{\gamma^2}\left[(1 - e^{\gamma}) + \frac{6(1 + e^{\gamma})}{\gamma} + \frac{24(1 - e^{\gamma})}{\gamma^2}\right]. \tag{A.8}$$

It can be checked directly that there is no singularity at $\gamma = 0$, such that both Eqs. (A.6) and (A.8) exist, and $\Phi_{p2}(0) = \Phi_{p4}(0) = 0$.

References

[1] Dynamic Interaction between Vehicles and Infrastructure Experiment (DIVINE), 1998, Technical Report, http://www.oecd.org/dsti/sti/transpor/road/prod/Free-on-line/DIVINE-rep.htm.

[2] R.J. Heywood, Influence of truck suspensions on the dynamic response of a short span bridge over Cameron's Creek, *International Journal of Vehicle Design, Heavy Vehicle Systems, Special Series* 3 (1996) 222–239.

[3] J.-W. Kou, J.T. DeWolf, Vibrational behavior of continuous span highway bridge—influencing variables, *American Society of Civil Engineers, Journal of Structural Engineering* 123 (1997) 333–344.

[4] L. Frýba, *Vibration of Solids and Structures under Moving Loads*, Thomas Telford, London, 1999.

[5] A.V. Pesterev, L.A. Bergman, C.A. Tan, Accurate model reduction in problems of bridge vibration due to moving vehicle, in: D.A. Indeitsev (Ed.), *Advanced Problems in Mechanics, Proceedings of the XXX Summer School*, Institute for Problems in Mechanical Engineering, Russian Academy of Sciences, St. Petersburg, 2003, pp. 522–529.

[6] M.F. Green, D. Cebon, Dynamic response of highway bridges to heavy vehicle loads: theory and experimental validation, *Journal of Sound and Vibration* 170 (1994) 51–78.

[7] G.T. Michaltos, T.G. Konstantakopoulos, Dynamic response of a bridge with surface deck irregularities, *Journal of Vibration and Control* 6 (2000) 667–689.

[8] K. Henchi, M. Fafard, M. Talbot, G. Dhatt, An efficient algorithm for dynamic analysis of bridges under moving vehicles using a coupled modal and physical components approach, *Journal of Sound and Vibration* 212 (1998) 663–683.

[9] Y.-B. Yang, B.-H. Lin, Vehicle–bridge interaction analysis by dynamic condensation method, *American Society of Civil Engineers, Journal of Structural Engineering* 121 (1995) 1636–1643.

[10] X.Q. Zhu, S.S. Law, Dynamic load on continuous multi-lane bridge deck from moving vehicles, *Journal of Sound and Vibration* 251 (2002) 697–716.

[11] A.V. Pesterev, L.A. Bergman, C.A. Tan, A novel approach to the calculation of pothole-induced contact forces in MDOF vehicle models, *Journal of Sound and Vibration* 275 (2004) 127–149.

[12] D.J. Cole, D. Cebon, Truck suspension design to minimize road damage, *Proceedings of the Institution of Mechanical Engineers Part D, Journal of Automobile Engineering* 210 (1996) 95–107.

[13] D.J. Cole, Fundamental issues in suspension design for heavy road vehicles, *Vehicle System Dynamics* 35 (2001) 319–360.

[14] T.D. Gillespie, Heavy Truck Ridde, SAE Special Publication SP 607, 1985.
[15] T.E.C. Potter, D. Cebon, D.J. Cole, Assessing 'road-friendliness': a review, *Proceedings of the Institution of Mechanical Engineers Part D, Journal of Automobile Engineering* 211 (1997) 455–475.
[16] B. Yang, Integral formulas for non-self-adjoint distributed dynamic systems, *American Institute of Aeronautics and Astronautics Journal* 34 (1996) 2132–2139.
[17] A.V. Pesterev, L.A. Bergman, C.A. Tan, Pothole-induced contact forces in a simple vehicle model, *Journal of Sound and Vibration* 256 (2002) 565–572.